Reaction Mechanisms

DOI: 10.1002/ange.201406823

Kinetic, Spectroscopic, and Theoretical Assessment of Associative and Dissociative Methanol Dehydration Routes in Zeolites**

*Andrew J. Jones and Enrique Iglesia**

Abstract: *Mechanistic interpretations of rates and in situ IR spectra combined with density functionals that account for van der Waals interactions of intermediates and transition states within confining voids show that associative routes mediate the formation of dimethyl ether from methanol on zeolitic acids at the temperatures and pressures of practical dehydration catalysis. Methoxy-mediated dissociative routes become prevalent at higher temperatures and lower pressures, because they involve smaller transition states with higher enthalpy, but also higher entropy, than those in associative routes. These enthalpy–entropy trade-offs merely reflect the intervening role of temperature in activation free energies and the prevalence of more complex transition states at low temperatures and high pressures. This work provides a foundation for further inquiry into the contributions of H-bonded methanol and methoxy species in homologation and hydrocarbon synthesis reactions from methanol.*

Rates of chemical reactions depend on free energy differences between transition states and their precursors. The functional form of Gibbs free energies favors enthalpic over entropic stabilization of transition states at modest temperatures.[1] These enthalpy–entropy trade-offs are evident, as shown herein, in causing methanol dehydration to dimethyl ether (DME) to proceed by direct (associative) instead of sequential (dissociative) routes at the low temperatures of its customary practice. Higher temperatures, relevant to the synthesis of hydrocarbons from methanol,[2] favor dissociative routes mediated by transition states with higher entropies but also higher enthalpies than for direct routes.

Two plausible catalytic CH_3OH dehydration sequences diverge after the quasi-equilibrated formation of H-bonded CH_3OH monomers at acidic OH (II, Scheme 1).[3] In associative routes, monomers react with CH_3OH(g) to form protonated CH_3OH dimers (Step D2, Scheme 1), which rotate to form the transition state (TS) for kinetically relevant DME formation steps (D4). In dissociative routes, CH_3OH dehydrates instead to form methoxy species in the kinetically relevant step (S2, Scheme 1); methoxy species then react with a CH_3OH(g) to form DME. The assumptions of pseudo-steady-state for adsorbed species and quasi-equilibrated monomers and dimers as the most abundant adsorbed intermediates (IR evidence presented below) give rate equations for associative routes:

$$\frac{r_{DME,D}}{[H^+]} = \frac{k_{D4}K_{D3}K_{D2}K_M[CH_3OH]^2}{K_M[CH_3OH] + K_{D2}K_M[CH_3OH]^2} = \frac{k_{D4}K_{D3}K_{D2}[CH_3OH]}{1 + K_{D2}[CH_3OH]} \quad (1)$$

and for their dissociative counterparts:

$$\frac{r_{DME,S}}{[H^+]} = \frac{k_{S2}K_M[CH_3OH]}{K_M[CH_3OH] + K_{D2}K_M[CH_3OH]^2} = \frac{k_{S2}}{1 + K_{D2}[CH_3OH]} \quad (2)$$

with rate and equilibrium parameters defined in Scheme 1 (derivations are given in the Supporting Information). Kinetically relevant steps are confirmed by density functional theory (DFT) below and elsewhere.[3a–c] TS theory formalisms give the ratio of these two rates (pressure units are those for free energy standard states for gaseous species; details in SI):

$$\frac{r_{DME,D}}{r_{DME,S}} = \exp\left(\frac{-(\Delta G_D^{\ddagger} - \Delta G_S^{\ddagger})}{k_B T}\right)\frac{[CH_3OH]}{1\ \text{bar}} = \chi. \quad (3)$$

These free energies represent those for the transition states involved in associative (direct, $\Delta G_D^{\ddagger}$) and dissociative (sequential, $\Delta G_S^{\ddagger}$) routes relative to gaseous reactants and the free Brønsted acid. Equation (3) accounts for the relative contributions of associative and dissociative routes at each temperature and CH_3OH pressure. These Gibbs free energies can be expressed in terms of the enthalpies and entropies of transition states relative to gaseous reactants and an unperturbed proton:

$$\Delta G_D^{\ddagger} - \Delta G_S^{\ddagger} = (\Delta H_D^{\ddagger} - \Delta H_S^{\ddagger}) - T(\Delta S_D^{\ddagger} - \Delta S_S^{\ddagger}) \quad (4)$$

DFT and statistical mechanics treatments have shown that associative (direct) dehydration routes prevail on W-based polyoxometalates (POM) at 400–500 K and 0.01–1 kPa CH_3OH pressures.[3a] Turnover rates on H-MFI increased linearly with CH_3OH pressure at low CH_3OH pressures,[4] which is consistent with Equation (1) but not with Eq. (2) when H-bonded CH_3OH monomers are the predominant surface species, as shown by the prevalence of their IR bands on H-MFI at sub-stoichiometric coverages (<1 CH_3OH per H^+);[5] such IR spectra were measured at (ambient) temperatures where dehydration is not detectable. Removing

[*] A. J. Jones, Prof. E. Iglesia
Department of Chemical and Biomolecular Engineering
University of California at Berkeley
Berkeley, CA 94720 (USA)
E-mail: Iglesia@berkeley.edu
Homepage: http://iglesia.cchem.berkeley.edu/

[**] We thank Dr. David Hibbitts (UC Berkeley) for helpful discussions, Chevron for financial support, and the XSEDE Science Gateways program (CTS130011) and the Environmental Molecular Sciences Laboratory of the Pacific Northwest National Laboratory for computational resources.

Supporting information for this article is available on the WWW under http://dx.doi.org/10.1002/anie.201406823.

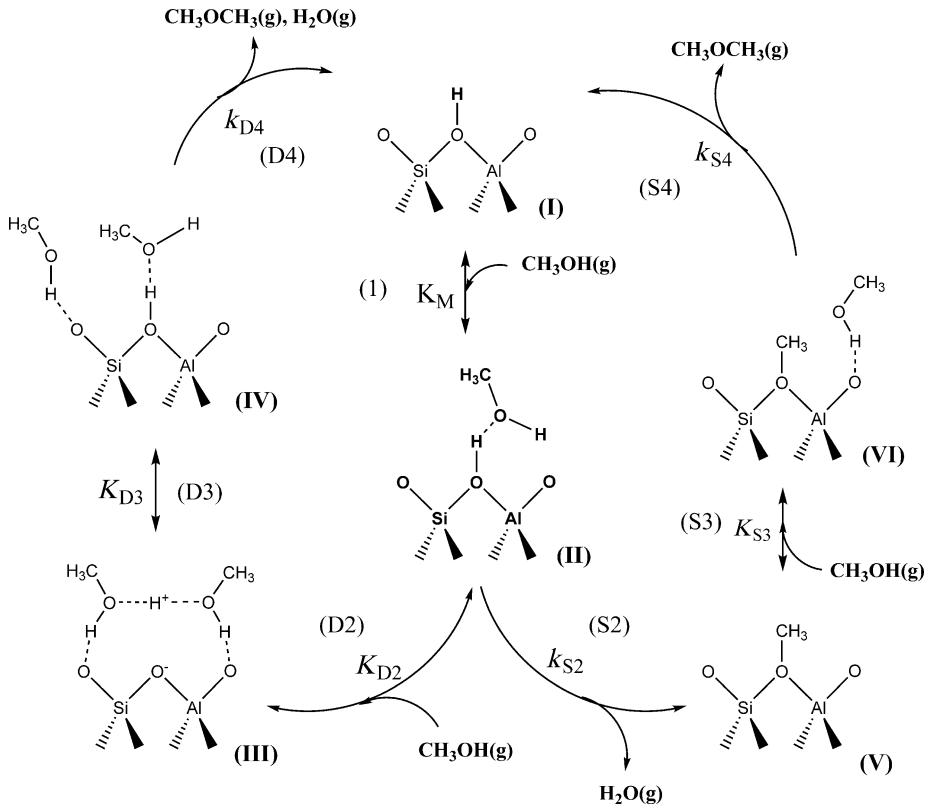

Scheme 1. Elementary steps for direct (associative; left cycle) and sequential (dissociative; right cycle) CH_3OH dehydration routes.

gaseous CH_3OH or DME leads to the detection of methoxy species by their IR[6] and ^{13}C MAS NMR[7] spectra; they can react with CH_3OH to form DME at 433–473 K.[8] These stoichiometric cycles are analogous to dissociative routes, but are limited to one turnover. An assessment of the contributions from dissociative and associative routes requires rate equations and IR spectra at conditions of dehydration catalysis.

Here, CH_3OH dehydration turnover rates and IR spectra are measured at relevant temperatures and CH_3OH pressures to assess the contributions of these two routes to DME formation rates. Periodic DFT methods with functionals that describe van der Waals interactions[9] are used here to assign IR bands and to extend this assessment to temperatures inaccessible to experiments because of ubiquitous side reactions.

The detection of O–H IR bands in zeolites and their perturbation or attenuation by H-bonded or protonated species, respectively, are rendered feasible by their sharp and isolated character (for example, 3604 cm^{-1} in H-MFI; Figure 1). Their frequencies are those expected for ν(OH) stretches in Brønsted acids (3621 cm^{-1} from DFT; Al12-O20(H)-Si3 in H-MFI henceforth). Contact with CH_3OH at catalytic conditions (0.2 kPa; 433 K) led to a broad band at 2371 cm^{-1} (Figure 1), corresponding to O–H groups perturbed by strong H-bonds with CH_3OH (2383 cm^{-1}; DFT). A band at 3581 cm^{-1}, absent from H-MFI or CH_3OH(g) spectra (Figure 1), appears during CH_3OH reactions and corresponds to ν(OH) modes in CH_3OH species interacting with framework O-atoms (3552 cm^{-1}; DFT). The 2620 cm^{-1} band appears at CH_3OH pressures of more than 0.5 kPa and becomes stronger with increasing pressure (Figure 2), which is consistent with higher coverages of protonated CH_3OH dimers (ν(OH) of dimers is 2608 cm^{-1} from DFT). Methyl deformation modes of methoxy species (1458 cm^{-1}; DFT) were not detected (0.2–16 kPa CH_3OH, 433 K) during steady-state catalysis, but emerge upon removal of CH_3OH(g) by evacuation at higher temperatures (1457 cm^{-1}; MFI; 523 K).[6b] Methoxy species are not present during catalysis at 433 K and 0.2–16 kPa CH_3OH, because H-bonded monomers are scavenged by CH_3OH(g) to form dimers before they can dissociate to methoxy species. Methoxy species can form, however, when CH_3OH(g) is removed and dimers can no longer form; H-bonded CH_3OH then either desorbs or forms stranded methoxy species and

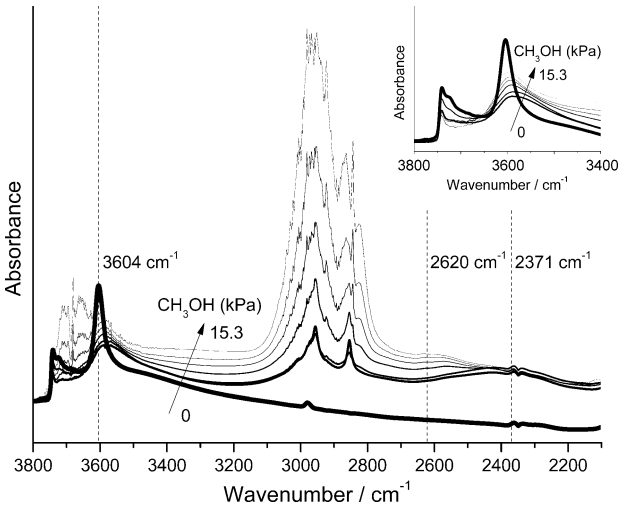

Figure 1. IR spectra of MFI (Si/Al = 43) with increasing CH_3OH pressure (0, 0.2, 0.5, 1.5, 3.8, 7.7, 15.3 kPa; dark to light) during steady-state dehydration reactions at 433 K. Inset: difference spectra to remove absorptions from gaseous CH_3OH.

H_2O(g). These spectra show that H-bonded monomers and protonated dimers (but neither unperturbed OH groups nor methoxy species) are the predominant species present at low (0.2–0.5 kPa) and high (7.7–16 kPa) CH_3OH pressures, respectively, and 433 K.

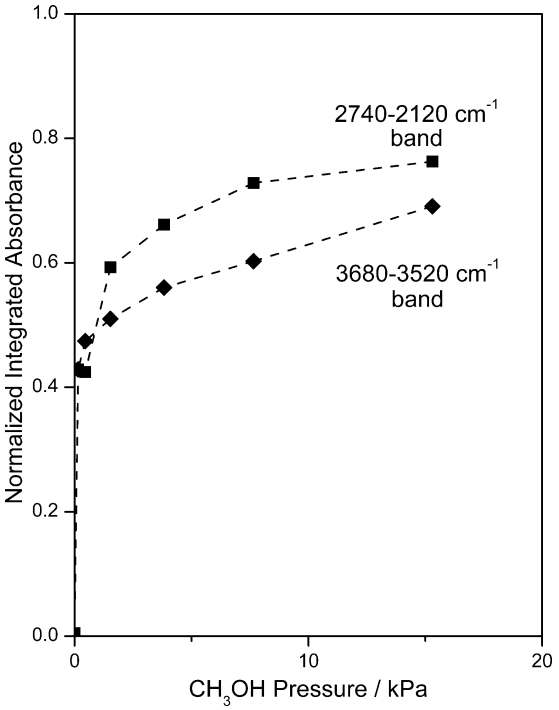

Figure 2. Integrated absorbance of IR bands characteristic of Brønsted ν(OH) from H-bonding with CH_3OH (2740–2120 cm^{-1}; ■) and CH_3OH ν(OH) perturbed by H-bonding (3680–3520 cm^{-1}; ◆) as a function of CH_3OH pressure normalized by the area of Si—O—Si overtone bands (2100–1730 cm^{-1}). Contributions of gaseous CH_3OH absorptions have been removed (for details, see the Supporting Information). Lines have been added to guide the eye.

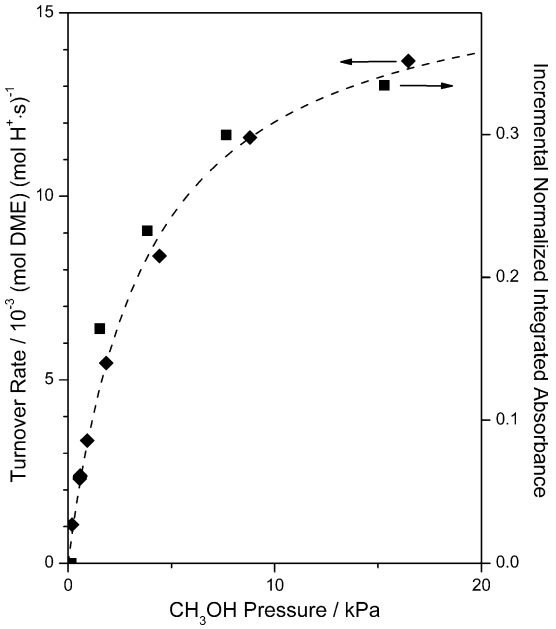

Figure 3. CH_3OH dehydration turnover rates (◆) and integrated IR absorbance of CH_3OH dimer ν(OH) perturbed by H-bonding (2740–2120 cm^{-1}; ■) normalized by the area of Si—O—Si overtone bands (2100–1730 cm^{-1}) as a function of CH_3OH pressure on MFI at 433 K. The absorbance data have been subtracted from the area of the same band at 0.5 kPa to remove contributions of gaseous CH_3OH.

Dehydration turnover rates (per H^+, from pyridine titration[4]) increased linearly with pressure at low pressures and then more gradually (Figure 3), as also observed on polyoxometalates and on MFI with Al, Ga, Fe, or B framework heteroatoms.[3a,4,10] Zero-order rate constants are similar on MFI samples with 0.05–10 μm crystals and 0.7–3.6 H^+ per unit cell (0.012–0.019 DME $(H^+s)^{-1}$, 433 K);[4] thus, diffusional constraints did not influence measured rates, which reflect the intrinsic reactivity of Brønsted acid sites within MFI.[4] These pressure effects on turnover rates reflect the prevalence of monomers at low pressures and of dimers at higher pressures; they cannot be described by dissociative (sequential) routes because these would lead to zero-order or negative-order reactions when monomers or dimers are predominant species, respectively [Eq. (2)]. The concurrent increase in turnover rates and the intensity of the IR band for dimers (normalized area of 2620 cm^{-1} band; Figure 3) is consistent with direct routes, because the rates of direct, but not sequential, routes are proportional to the number of such dimers (Scheme 1).

These results, taken together, demonstrate that associative routes (Scheme 1, left; Eq. (1)) prevail on MFI at typical conditions of dehydration catalysis, and by inference, on other zeolites (FAU, SFH, BEA, MTW, MOR, MFI, MTT) in light of their similar kinetic behavior.[10] Direct routes also prevail on the stronger acid sites of polyoxometalates (deprotonation energies of 1080–1143 kJ mol^{-1}[3a] vs. 1171–1205 kJ mol^{-1} on crystalline aluminosilicates[4,11]), because changes in acid strength influence the two free energy terms in Equation (3) to similar extents.[3a]

Activation entropies and enthalpies measured from temperature effects on dehydration rate constants are shown in Table 1 (Arrhenius plots are given in the Supporting Information). Enthalpy barriers for k_{first} ($k_{D4}K_{D3}K_{D2}$; $\Delta H^{\ddagger}_{first} = 42 \pm 2$ kJ mol^{-1}) are smaller than for k_{zero} ($k_{D4}K_{D3}$; $\Delta H^{\ddagger}_{zero} = 90 \pm 2$ kJ mol^{-1}), as expected from two effective barriers that reflect the enthalpy of the same TS but referenced to CH_3OH and CH_3OH(g) (for $\Delta H^{\ddagger}_{first}$) and to a more stable dimer (for $\Delta H^{\ddagger}_{zero}$). Activation entropies, in turn, are more negative for k_{first} ($\Delta S^{\ddagger}_{first} = -160 \pm 10$ J K^{-1} mol^{-1}) than for k_{zero} ($\Delta S^{\ddagger}_{zero} = -75 \pm 2$ J K^{-1} mol^{-1}) because the reference state for k_{first} has higher entropy. The corresponding enthalpies and entropies of activation for sequential routes cannot be measured accurately because

Table 1: Measured and calculated (vdW-DF2/PAW) enthalpic, entropic, and free energy barriers for CH_3OH dehydration at 433 K.[a]

	Measured	Calculated
$\Delta H^{\ddagger}_{first}$ [kJ mol^{-1}]	42 ± 2	10
$\Delta H^{\ddagger}_{zero}$ [kJ mol^{-1}]	90 ± 2	84
$\Delta S^{\ddagger}_{first}$ [J mol^{-1} K^{-1}]	−160 ± 10	−150
$\Delta S^{\ddagger}_{zero}$ [J mol^{-1} K^{-1}]	−75 ± 2	14
$\Delta G^{\ddagger}_{first}$ [kJ mol^{-1}]	111 ± 9	75
$\Delta G^{\ddagger}_{zero}$ [kJ mol^{-1}]	123 ± 3	78

[a] First-order and zero-order barriers refer to the energy of the direct transition state relative to CH_3OH monomers and CH_3OH(g), and CH_3OH dimers, respectively.

such routes become favored only at higher temperatures, which lead to diffusional corruptions, side reactions, rapid deactivation, and near-equilibrium CH_3OH conversions.

TS enthalpies and entropies can be estimated using periodic DFT methods with vdW-DF2 functionals[9] that include distinct terms (separable from local interactions) to account for van der Waals forces and H-bonds. Reaction coordinate diagrams for direct and sequential routes are shown in Figure 4. TS enthalpies for methoxy formation (TS2; relative to monomers) are 83 kJ mol^{-1} larger than for bimolecular dehydration (TS1; relative to monomers and CH_3OH(g); Figure 4a), reflecting the more effective enthalpic stabilization of TS1 over TS2 within zeolite voids. The van der Waals stabilization part of TS enthalpies is more negative (by 48 kJ mol^{-1}) for TS1 than for TS2 (relative to the same reference state), indicating that dispersive interactions preferentially stabilize the larger transition states in associative (TS1) routes.

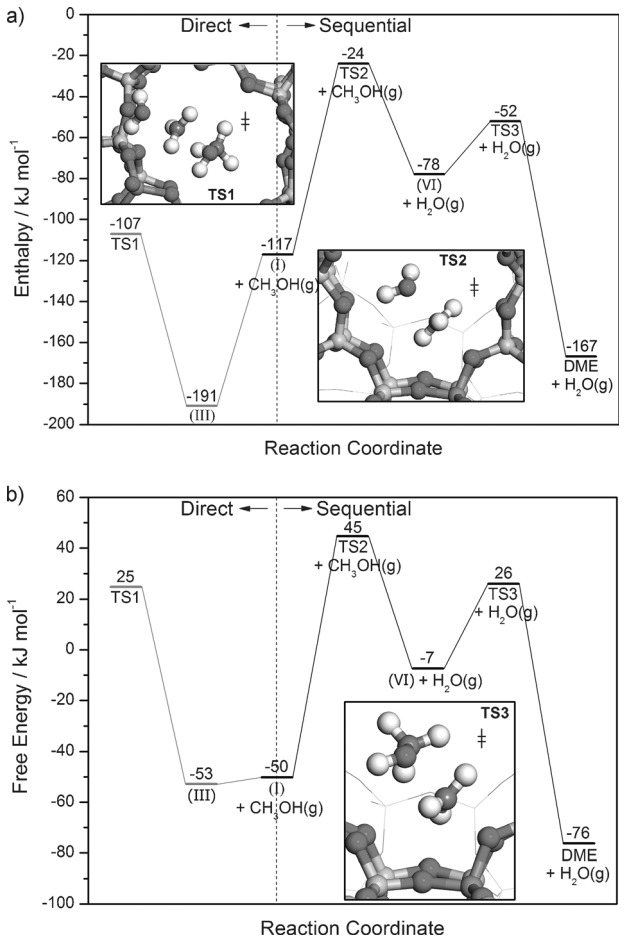

Figure 4. Enthalpies (a) and free energies (433 K; b) of structures shown in Scheme 1 involved in direct (associative) (left; gray) and sequential (dissociative) (right; black) routes on MFI at the Al12-O20(H)-Si3 location from DFT (vdW-DF2/PAW). Energies are relative to the bare zeolite and two CH_3OH(g).

Measured enthalpies of formation of DME formation transition states from dimers ($\Delta H^{\pm}_{zero}$) are similar to those derived from DFT (90 and 84 kJ mol^{-1}, respectively; Table 1), while those for that TS, but referenced to monomers and CH_3OH(g) ($\Delta H^{\pm}_{first}$) are 30 kJ mol^{-1} larger than DFT estimates. The difference between $\Delta H^{\pm}_{first}$ and $\Delta H^{\pm}_{zero}$ reflects the enthalpy of dimer formation by reaction of CH_3OH(g) with monomers and measured values (−48 kJ mol^{-1}) are less negative than those derived from DFT (−74 kJ mol^{-1}), most likely because the functional used overestimates van der Waals interactions.[12]

Entropies of transition states and relevant intermediates were calculated from DFT-derived frequencies using the harmonic approximation, which underestimates entropies for loosely bound species,[13] but is accurate for strongly bound species, such as the TS and monomers involved in CH_3OH dehydration.[3c] Measured TS1 entropies ($\Delta S^{\pm}_{first}$; −150 J K^{-1} mol^{-1}, Table 1) are similar to DFT-derived values (−158 J K^{-1} mol^{-1}, Table 1), but $\Delta S^{\pm}_{zero}$ estimates (14 J K^{-1} mol^{-1}) are much less negative than measured values (−75 J K^{-1} mol^{-1}) because the full translational and rotational freedom of protonated dimers is not captured by the harmonic potential. Experimental rate constants and barriers avoid the inaccuracies of DFT, however, DFT comparisons of direct and sequential routes are informative about the qualitative contributions of enthalpy and entropy to free energies.

The difference in TS free energies between direct and sequential routes in Equation (3) derived from DFT (vdW-DF2/PAW) enthalpies and entropies is −20 kJ mol^{-1} at 433 K (Figure 4b), which leads to direct-to-sequential rate ratios (χ, Eq. (3)) that increase from 0.5 to 40 at 433 K as the pressure increases from 0.2 to 16 kPa and to detectable contributions from dissociative routes only at the lowest pressures, which are much lower than used in dehydration catalysis practice. These χ values, taken together with the lack of detectable contributions from dissociative routes inferred from rate and IR data (even at 0.2 kPa), suggest that DFT methods may actually overestimate dissociative contributions. The DFT-derived (RPBE/PAW) TS free energy differences responsible for χ values (Eq. (3)) on TON zeolites at 433 K are 20 kJ mol^{-1},[3c] which lead to χ values of 0.0006 at 16 kPa; these calculations neglect dispersion forces, which account for 48 kJ mol^{-1} of the energy difference between TS1 and TS2 in MFI, and, when added, χ estimates from DFT become similar for TON and MFI.

DFT-derived CH_3OH dehydration rate constants for associative and dissociative routes are shown in Figure 5 as a function of temperature. Associative routes are preferred ($\chi > 1$) below 503 K at 0.1 bar CH_3OH and below 570 K at 1 bar CH_3OH (Figure 5). Dissociative route transition states (TS2) have more positive enthalpies and entropies than the TS1 that mediates associative routes, thus making the rate constants for the latter less sensitive to temperature than for dissociative routes (Figure 5). At the low-temperatures of CH_3OH dehydration catalysis, associative routes are favored, as shown by kinetic and IR data shown herein, while at higher temperatures typical of CH_3OH conversion to hydrocarbons (ca. 600 K), CH_3OH–DME interconversions become equilibrated and dissociation may occur, leading to the plausible involvement of methoxy species in methylation of alkenes at high temperatures.[2,14]

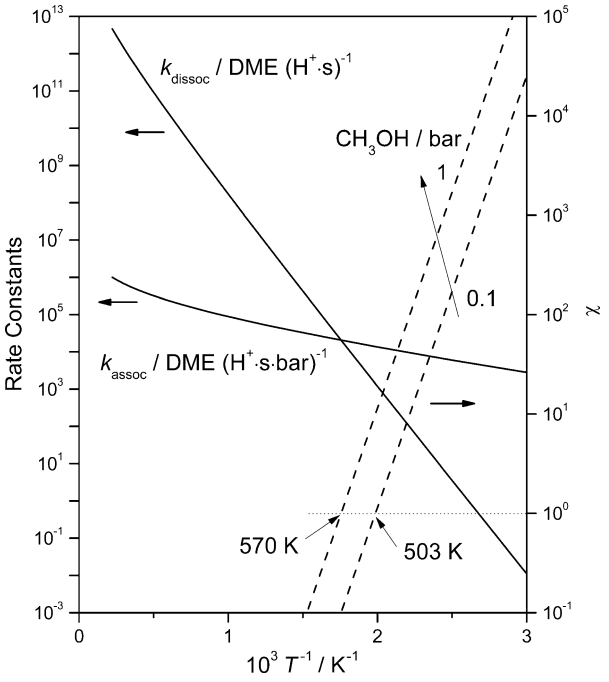

Figure 5. Associative ($k_{assoc} = k_{D4}K_{D3}K_{D2}$; Scheme 1) and dissociative ($k_{dissoc} = k_{S2}$) rate constants and the ratio of associative-to-dissociative rates (χ; dashed lines) determined from Equations (3) and (4) at 0.1 and 1 bar CH_3OH and estimated from DFT-derived enthalpies and entropies (vdW-DF2/PAW).

The preferred DME formation routes depend on CH_3OH pressure, because the stabilization of H-bonded monomers by dimer formation precludes their dissociation, and on temperature, because lower temperatures favor the more "complex" but lower-enthalpy TS that mediates associative routes. We surmise also that solvation by confinement within voids similar in size to the associative TS may enhance their contribution to measured DME formation rates, while dissociative routes may become prevalent for voids too small to contain associative TS, but able to solvate those involved in methoxy formation (and still fit the TS for the subsequent CH_3OH–methoxy complex in dissociative routes). For larger voids, including mesoporous structures, associative routes predominate at conditions of practical methanol dehydration catalysis.

Experimental Section

H-MFI (Zeolyst, Si/Al = 43) and the experimental methods for measuring turnover rates and H^+ density are discussed elsewhere.[4] Activation energies and pre-exponential factors were determined from rate constants measured as a function of temperature (414–475 K; Supporting Information). The experimental setup for IR spectroscopy is described elsewhere;[4] liquid CH_3OH (99.8%, Sigma–Aldrich) was introduced to flowing He (333 $cm^3 g^{-1} s^{-1}$, 99.999%, Praxair) by a syringe pump (Cole-Palmer 780200C series) into heated stainless steel lines (373 K) that connect to a quartz cell with NaCl windows. Periodic plane-wave DFT calculations were performed with projector augmented-wave potentials,[15] an energy cutoff of 396 eV, and the vdW-DF2[9] functional implemented in the Vienna ab initio simulation package (Supporting Information).[16] Wavefunctions were converged to within 10^{-6} eV. Structures were relaxed until the forces on all atoms were < 0.05 eVA^{-1}. TS structures were obtained from the nudged elastic band[17] and dimer[18] methods.

Received: July 2, 2014
Published online: September 11, 2014

Keywords: density functional calculations · dimethyl ether · hydrogen bonding · methanol · IR spectroscopy

[1] R. Gounder, E. Iglesia, *Acc. Chem. Res.* **2012**, *45*, 229–238.
[2] M. Stöcker, *Microporous Mesoporous Mater.* **1999**, *29*, 3–48.
[3] a) R. T. Carr, M. Neurock, E. Iglesia, *J. Catal.* **2011**, *278*, 78–93; b) S. R. Blaszkowski, R. A. vanSanten, *J. Phys. Chem. B* **1997**, *101*, 2292–2305; c) P. G. Moses, J. K. Norskov, *ACS Catal.* **2013**, *3*, 735–745; d) S. R. Blaszkowski, R. A. vanSanten, *J. Am. Chem. Soc.* **1996**, *118*, 5152–5153.
[4] A. J. Jones, R. T. Carr, S. I. Zones, E. Iglesia, *J. Catal.* **2014**, *312*, 58–68.
[5] A. Zecchina, S. Bordiga, G. Spoto, D. Scarano, G. Spano, F. Geobaldo, *J. Chem. Soc. Faraday Trans.* **1996**, *92*, 4863–4875.
[6] a) P. Salvador, W. Kladnig, *J. Chem. Soc. Faraday Trans. 1* **1977**, *73*, 1153–1168; b) H. Yamazaki, H. Shima, H. Imai, T. Yokoi, T. Tatsumi, J. N. Kondo, *Angew. Chem. Int. Ed.* **2011**, *50*, 1853–1856; *Angew. Chem.* **2011**, *123*, 1893–1896.
[7] W. Wang, A. Buchholz, M. Seiler, M. Hunger, *J. Am. Chem. Soc.* **2003**, *125*, 15260–15267.
[8] a) W. Wang, M. Hunger, *Acc. Chem. Res.* **2008**, *41*, 895–904; b) H. Yamazaki, H. Shima, H. Imai, T. Yokoi, T. Tatsumi, J. N. Kondo, *J. Phys. Chem. C* **2012**, *116*, 24091–24097.
[9] K. Lee, É. D. Murray, L. Kong, B. I. Lundqvist, D. C. Langreth, *Phys. Rev. B* **2010**, *82*, 081101.
[10] A. J. Jones, S. Zones, E. Iglesia, *J. Phys. Chem. C* **2014**, *118*, 17787–17800.
[11] M. Brändle, J. Sauer, *J. Am. Chem. Soc.* **1998**, *120*, 1556–1570.
[12] F. Göltl, A. Grüneis, T. Bučko, J. Hafner, *J. Chem. Phys.* **2012**, *137*, 114111.
[13] a) T. Bucko, J. Hafner, *J. Phys. Condens. Matter* **2010**, *22*, 384201; b) T. Bučko, L. Benco, J. Hafner, J. G. Ángyán, *J. Catal.* **2011**, *279*, 220–228.
[14] U. Olsbye, S. Svelle, M. Bjørgen, P. Beato, T. V. W. Janssens, F. Joensen, S. Bordiga, K. P. Lillerud, *Angew. Chem. Int. Ed.* **2012**, *51*, 5810–5831; *Angew. Chem.* **2012**, *124*, 5910–5933.
[15] a) G. Kresse, D. Joubert, *Phys. Rev. B* **1999**, *59*, 1758–1775; b) P. E. Blöchl, *Phys. Rev. B* **1994**, *50*, 17953–17979.
[16] a) G. Kresse, J. Furthmüller, *Phys. Rev. B* **1996**, *54*, 11169–11186; b) G. Kresse, J. Hafner, *Phys. Rev. B* **1993**, *47*, 558–561.
[17] G. Henkelman, H. Jónsson, *J. Chem. Phys.* **2000**, *113*, 9978–9985.
[18] G. Henkelman, H. Jónsson, *J. Chem. Phys.* **1999**, *111*, 7010–7022.

